New insights into the composition of Indian yellow and its use in a Rajasthani wall painting

Diego Tamburini [(1)]*, Charlotte Martin de Fonjaudran [(2)], Giovanni Verri [(2)], Gianluca Accorsi [(3)], Angela Acocella [(4)], Francesco Zerbetto [(4)], Amarilli Rava [(2)], Samuel Whittaker [(2)], David Saunders [(1)], Sharon Cather [(2)]

[(1)] Department of Scientific Research, The British Museum, Great Russell Street, London WC1B 3DG, UK
[(2)] The Courtauld Institute of Art, Somerset House, Strand, WC2R 0RN, London, UK,
[(3)] CNR NANOTEC - Institute of Nanotechnology c/o Campus Ecotekne, University of Salento; Via Monteroni - 73100 Lecce, Italy.
[(4)] Department of Chemistry "G.Ciamician", University of Bologna, Via F. Selmi 2, 40126, Bologna, Italy

* Correspondence should be addressed to Dr. Diego Tamburini
Email: Dtamburini@britishmuseum.org ; Tel +44 02073238123

Abstract

The widespread occurrence of Indian yellow on an early 17th-century wall painting in Rajasthan (India) was initially indicated by photo-induced luminescence imaging of the painted scheme in the Badal Mahal within the Garh Palace (Bundi). The presence of the organic pigment was subsequently confirmed by HPLC-ESI-Q-ToF. The results of a multi-analytical study focusing on two samples from the wall painting and two reference pigments from the British Museum and National Gallery (London, UK) are presented here. The research focused on the possible causes for the different yellow/orange hues observed in the painting samples.
Analysis of cross-sections with SEM-EDS revealed similar elemental composition for the Indian yellow paint layers, but different underlying layers, indicating a variation in painting technique. The composition of the Indian yellow samples was investigated by HPLC-ESI-Q-ToF with both positive and negative ionisation. In addition to euxanthic acid and euxanthone, a sulphonate derivative of euxanthone was found to be present in all samples, while relative amounts of the three components varied. Flavonoid molecules—morin, kaempferol, quercetin and luteolin—were also detected in one wall painting sample (characterised by a brighter yellow colour) and not in the sample that was more orange.

The optical properties of the samples were characterised by photoluminescence spectroscopy in both solid state and aqueous solution. The contribution of each organic compound to the emission spectrum of Indian yellow in solution was also investigated by time-dependent density functional theory (TDDFT) calculations. Small differences in terms of spectral shift were observed in solid state experiments, but not in solution, suggesting that the spectral differences in the emission spectrum were mostly due to different contributions of solid-state arrangements, most likely driven by π- π stacking and/or hydrogen bonds. However, a slight difference at high energies was observed in the spectra acquired in solution and TDDFT calculations permitted this to be ascribed to the different chemical composition of the samples. Time-resolved measurements highlighted di-exponential lifetime decays, confirming the presence of at least two molecular arrangements. Py(HMDS)-GC-MS was also used for the first time to characterise Indian yellow and the trimethylsilyl derivative of euxanthone was identified in the pyrograms, demonstrating it to be a suitable marker for the identification of the pigment in complex historic samples.

Keywords: Indian yellow; SEM-EDS; photoluminescence; HPLC-MS; Py-GC-MS; wall painting

1. Introduction

The widespread occurrence of Indian yellow, a pigment described as a mixture of the magnesium and calcium salts of euxanthic acid [1, 2], on the early 17th-century wall paintings in the Badal Mahal ('Cloud Palace') within the Garh Palace in Bundi (Rajasthan, India) was previously reported by the authors [3]. The painted scheme, dated to 1620-30 CE, is one of the earliest, finest and most complete surviving wall paintings illustrating the artistic patronage of Bundi rulers at that time [4]. The daily life of royal figures is associated with scenes of Hindu mythology centred on Krishna (Figure 1). While Indian yellow is often found on Rajput-Mughal miniature paintings from the late 16th to the 19th century [5, 6], its use in wall paintings was previously unknown. The production method of Indian yellow has been debated since the 19th century but conclusions from the exhaustive review by Ploeger *et al.* [7] points towards the likelihood of a metabolic production pathway involving the collection of urine from cows fed solely on mango leaves, as already reported by Mukharji in the 19th century [8].

Most published studies of Indian yellow have centred on its identification in works of art [5, 9-13], but detailed investigations of the physical and chemical characteristics of this organic pigment are rare [3]. However, there is evidence that its description as a mixed Ca and Mg salt of euxanthic acid is over-simplistic. In particular, euxanthone, the aglycone product of

euxanthic acid, is reported to occur alongside the acid [1, 10], and a sulphonate derivative of euxanthone has been recently identified [3]. The relative abundances of these components, both in terms of the ratio of euxanthone to euxanthic acid and the concentrations of Ca and Mg, have been reported to vary considerably and it has been speculated that they relate to the purity of the pigment [1]. This variability also appeared to have an influence on the photophysical properties of the material [3], but other factors may play a role, such as the mean crystal size of the particles. The final outcome of these differences is that Indian yellow pigments sometimes show different yellow hues.

In this study we decided to investigate further the possible causes for the variations in the optical characteristics of Indian yellow, as the two samples collected from the wall painting showed slightly different colours.

Most analytical techniques are increasingly being adapted to offer portability and non-invasiveness (XRF, FTIR, Raman) [14-16] and, when combined with imaging techniques [12, 17-20], can provide very useful information, leading to the identification of materials and aiding in their condition assessment. However, when micro-samples can be taken, the level of detailed chemical information that can be obtained increases significantly, especially for organic materials: the observation and analysis of cross-sections (SEM-EDS) [21, 22] coupled with chromatographic analysis (GC-MS, HPLC-MS, Py-GC-MS) [23] is a powerful combination. When these are integrated with analytical methods that are capable of providing information on both the chemical nature and physical characteristics of materials (steady-state and time-resolved photoluminescence spectroscopy) [24-26], the information obtained is yet more comprehensive.

For these reasons, a wide array of techniques was adopted for this study: photo-induced luminescence (PL) imaging and spectroscopy, SEM-EDS, HPLC-MS and Py(HMDS)-GC-MS were applied to investigate the samples from both the wall painting and the reference materials. TDDFT calculations were also used to integrate and confirm some information, as they focused on the contribution of each organic compound to the emission spectrum of Indian yellow and they enabled the emission spectra of the samples to be simulated in aqueous solution. This research highlights the complementary roles played by these analytical and theoretical techniques in bringing new insights into the chemical composition and photophysical properties of Indian yellow.

2. Materials and methods

2.1 Samples

The wall painting samples were taken from two different locations on the south wall of the Badal Mahal (Figure 2). Sample S63 was characterised by a lemon yellow paint layer,

whereas sample S64 showed a deeper orange-yellow paint layer. Both yellows are extensively used for the geometrical and floral patterns present across the wall. Powdered reference samples of Indian yellow were acquired from the pigment archives of the British Museum (BM) and the National Gallery (NG) in London (see Figure 3). Unfortunately, no information on the provenance or age of the BM and NG reference compounds is available.

2.2 Photoluminescence (PL) imaging

The equipment and protocol for PL imaging of the painted scheme is described in Martin de Fonjaudran *et al*. [3]. Further characterisation of the PL properties of the BM and NG reference samples was performed using a customised Nikon D7000 camera, which records emission in the *c.* 350-1100 nm spectral range. The excitation source consisted of two modified Metz Mecablitz 76 MZ-5 xenon flashtubes at their highest output settings [27]. The modification consisted of the removal of the plastic diffuser and its replacement with a filter holder. The excitation and emission ranges were therefore selected by placing bandpass filters in front of the xenon flashtube and camera lens, respectively. The filters used for UV-induced luminescence in the visible (UV-VISL) and IR ranges (UV-IRL), and visible-induced luminescence in the IR range (VIS-IRL) are summarised in Table 1.

The NG and BM samples were placed in a non-luminescent metal holder above a uniform, non-luminescent black surface. A uniform, flat white board covering the entire field of view, a Gretag-Macbeth ColorChecker chart, and a set of lambertian reflectance standards (Spectralon® 99, 50, 25 and 12.5%) were inserted in all images to allow for post-capture processing and correction (light distribution, colour correction, removal of ambient stray reflected light). All images were then processed and corrected using Nip2 software following the protocol described in Dyer *et al*. [28].

2.3 Optical microscopy

The wall painting samples were embedded in polyester resin and polished to reveal their stratigraphy. Cross-sections were imaged under normal and UV illumination with a Leica DMRX optical microscope equipped with 10x and 20x PL Fluotar objectives. For UV examination, a mercury light source and a filter cube, with excitation filter BP 340-380 nm, dichroic mirror RKP 400 nm and suppression filter LP 425 nm, were used.

2.4 SEM-EDS

The cross-sections were observed uncoated using a Hitachi S-3700N variable pressure (VP) scanning electron microscope. Analysis was performed at low vacuum (40 Pa), 15-20 kV

accelerating voltage, with an initial 10 mm working distance. The back-scattered electron (BSE) detector was used in the compositional (COMP) mode.

Elemental maps were acquired over four hours on selected areas using 2048 x 2048 resolution, 0-20 eV energy range and 50 ms dwell time. AZtecEnergy analysis software (Oxford Instruments) was used to process the data and reconstruct the EDS spectra.

2.5 Photophysical properties

Emission and excitation spectra were recorded with an Edinburgh FLS980 spectrometer equipped with a Peltier-cooled Hamamatsu R928 photomultiplier tube (185-850 nm) and a Xenon Lamp (450 W) as light source. The emission lifetimes in the pico- to nanosecond timescale were measured using a single photon counting system (Edinburgh FLS980 spectrometer) with a 1 MHz laser diode as excitation source coupled with a Hamamatsu MCP R3809U-50, time resolution 20 ps, as detector. The level of confidence is estimated to be ± 8% for τ determinations.

2.6 TDDFT calculations

The optical properties of the pigment in aqueous solution were investigated in terms of their molecular components, focusing on the photophysical properties of the first $^1(\pi_H \rightarrow \pi_L^*)$ excited state. In an attempt to resolve the emission spectra of Indian yellow samples in solution, quantum mechanical calculations in water were carried out, on the ground and the first $^1(\pi_H \rightarrow \pi_L^*)$ singlet excited states of euxanthone (E), euxanthone sulphonate (SE) and euxanthic acid (EA).

All the calculations were performed using DFT [29] and its time-dependent extension, TDDFT [30-32], as implemented in the Gaussian09 suite of packages [33], at the B3LYP/TZVP level of theory [34]. The exchange-correlation functional and basis set used were those selected from the benchmarking analysis run in our previous work to reproduce absorbance properties in a vacuum and in water for the same chromophores [3]. Solvent effects were then introduced by means of the CPCM polarisable conductor model implemented in Gaussian09 [35, 36], with the Pauling cavity set [37] and optimisation of the excited states in water performed using a classical linear-response (LR-CPCM) approach [38, 39]. In order to obtain a more accurate description of the solvent effect in water, the solvent reaction field was also taken into account using, on the optimised LR-CPCM geometries, the state-specific self-consistent procedure model (SS-CPCM), [40, 41], one of the most accurate models yet developed to take into account the variation of the solvent polarisation.

The vibrationally-resolved emission spectra were calculated by means of the Franck-Condon (FC) approximation, within the adiabatic Hessian approach, implemented in Gaussian09. This model requires a large computational effort, as the vibrational frequencies of the optimised ground and excited state geometries need to be calculated, analytically and numerically respectively.

2.7 HPLC-ESI-Q-ToF

A combined mild extraction procedure was adopted in this study. Approximately 0.1 mg of sample was admixed with 200 µL DMSO and heated at 80°C for 10 minutes. After centrifugation, the supernatant was transferred into another vial. The residue was admixed with 200 µL of methanol/acetone/water/0.5M oxalic acid 30:30:40:1 (v/v/v/v) at 80°C for 15 minutes. The solution was evaporated under N_2 and reconstituted using 200 µL of 1:1 MeOH/H_2O (v/v). The DMSO extract was combined with the oxalic acid extract and the solution was centrifuged for 10 minutes. The supernatant was transferred to a fresh 250 µL insert and 5-10 µL of the solution were injected into the HPLC system.

Analyses were carried out using a 1260 Infinity HPLC (Agilent Technologies), coupled to a 1100 DAD detector (Hewlett-Packard) and a Quadrupole-Time of Flight tandem mass spectrometer with a 6530 Infinity Q-ToF detector (Agilent Technologies) by a Jet Stream ESI interface (Agilent Technologies).

The HPLC conditions were: Zorbax Extend-C18 column (2.1 mm × 50 mm, 1.8 µm particle size); 0.4 mL·min^{-1} flow rate; 5 µL injection volume for MS experiments and 10 µL for MSMS experiments; 40°C column temperature. Separation was achieved using a gradient of water with 0.1% formic acid (eluent A) and acetonitrile with 0.1% formic acid (eluent B). The elution gradient was programmed as follows: initial conditions 95% A, followed by a linear gradient to 100% B in 10 min, then held for 2 min. Re-equilibration time for each analysis was 10 min. The ESI operating conditions were: drying gas (N_2, purity >98%): 350°C and 10 L·min^{-1}; capillary voltage 4.0 kV; nebulizer gas 276 kPa; sheath gas (N_2, purity >98%): 375°C and 11 L·min^{-1}.

High resolution MS and MS/MS spectra were acquired in negative and positive modes in the range 100-1700 m/z. The fragmentor was kept at 150 V, nozzle voltage 1000 V, skimmer 65 V, octapole RF 750 V. For the MS/MS experiments, different voltages in the collision cell were tested for Collision Induced Dissociation (CID), in order to maximise the information obtained from fragmentation. The collision gas was nitrogen (purity 99.999%). The data were collected by targeted MS/MS acquisition with an MS scan rate of 1.0 spectra per second and an MS/MS scan rate of 1.0 spectra per second. MassHunter® Workstation Software was used to carry out mass spectrometer control, data acquisition and data analysis.

2.8 Py(HMDS)-GC-MS

Analytical pyrolysis was performed using 1,1,1,3,3,3-hexamethyldisilazane (HMDS, chemical purity 99.9%, Sigma Aldrich Inc., USA) as a silylation agent for the *in situ* thermally-assisted derivatisation of pyrolysis products. The instrumentation consisted of a 1500 CDS Pyroprobe 1000 Series filament pyrolyser (CDS Analytical, USA) (platinum coil) coupled to a gas chromatograph 6890 (Agilent Technologies, USA) equipped with an HP-5MS fused silica capillary column (30 m × 0.25 mm i.d., 0.25 µm thickness, Agilent Technologies, USA). The GC was coupled with an Agilent 5973 Mass Selective Detector operating in electron impact mode (EI) at 70 eV. Pyrolysis temperatures of 400, 500 and 600°C were tested on reference samples and the interface temperature was 275°C. A pyrolysis temperature of 500°C was adopted for the wall painting samples. Similar amounts (*c.*100 µg) of sample and HMDS (2 µL) were inserted into the centre of the pyrolysis quartz tube with quartz wool and then put into the filament coil. The GC injector was used with a split ratio of 1:10 at 300°C. Chromatographic conditions were as follows: initial temperature 36°C, 10 min isothermal, 10°C·min^{-1} up to 280°C, 2 min isothermal; 20°C·min^{-1} up to 310°C, 50 min isothermal. Helium (purity 99.995%) was used as carrier gas with a constant flow of 1.0 mL·min^{-1}.

3. Results

3.1 Photoluminescence imaging

Photoluminescence imaging of the wall painting has been described previously in Martin de Fonjaudran *et al.* [3] but is briefly presented here to provide context for these additional investigations. Figure 3 (top) shows the visible (right), UV-VISL (middle) and UV-IRL (left) images of the overall area from which sample S64 was taken. Sample S64 is characterised by a yellow-orange colour in the visible image and a deep orange fluorescence in the UV-VISL image (excitation *c.*280-400 nm and emission *c.*400-700 nm). Practical limitations of *in situ* capture of PL images prevented the photoluminescence at the exact site of sample S63 from being recorded; however, *in-situ* observations revealed similar PL properties elsewhere in the painting scheme to the second yellow illustrated in Figure 3, characterised by a paler colour in the visible image and a bright yellow fluorescence in the UV-VISL image. Both yellows show strong emissions in the IR range and appear ‘glowing white’ against a dark grey background in the UV-IRL image (excitation *c.* 280-400 nm and emission *c.*700-1000 nm).

A more exhaustive PL imaging sequence was performed for BM and NG reference samples. Figure 3 (bottom) illustrates the UV-VISL, UV-IRL and VIS-IRL properties of both reference samples (see Table 1 for details on excitation and emission wavelengths). Post-capture image corrections allowed reliable comparison of colour and photoluminescence intensity

between both samples. The colour of both samples is only slightly different in the visible range: the BM sample appears more yellow and the NG sample more orange. Comparing their overall emissions, although the two are similar, the NG sample differs in that it shows a stronger emission in the IR spectral range above 830 nm following UV excitation (see UV-IRL2).

3.2 Optical microscopy and SEM-EDS

The cross-sections of samples S63 and S64 (Figure 4) revealed that the two areas of the painting were executed using different techniques. In sample S63, the yellow paint layer was applied directly on the lime-based plaster, whereas sample S64 showed a preparation/ground layer between the lime-based plaster and the paint layer, clearly visible in the SEM-EDS maps (Figure 5). FTIR analysis of samples of the plaster (not reported here), showed that it is of dolomitic origin ($CaMg(CO_3)_2$). This result was in agreement with EDS analysis, which revealed the presence of Ca and Mg in the plaster layer. Si, Al and traces of K, possibly corresponding to the use of clays, were present as the most abundant elements in the ground/preparation layer of sample S64. Some particles containing lead were also detected by EDS in the white preparation layer. Lead might have been naturally present in the material or added as lead white or as another lead-containing material. When observed at high magnification under UV radiation, S64 appeared to be composed of an orange matrix, in which small bright yellow particles were embedded. This was not observed for sample S63, which showed a more homogeneous distribution of the bright yellow emission. The mean size of the particles was difficult to measure, especially because some larger particles were found to be agglomerates of smaller particles. Nevertheless, as a general observation, finer particles with a more homogeneous distribution were observed in sample S63, whereas larger particles (up to 30 µm) were present in sample S64. This may be related to different methods of manufacture of the pigments, resulting in slightly different colour shades. However, the areas corresponding to particles with different colours did not correspond to any variation in elemental composition, as highlighted in the SEM-EDS images (Figure 4).

The paint layer showed the presence of Mg and Ca, in agreement with the composition of Indian yellow [1]. In both samples, Mg appeared to be relatively more abundant and more homogeneously distributed than Ca, which seemed to be more concentrated in specific areas. However, these areas do not correlate with the presence of other specific elements or colours. A similar distribution of Ca and Mg, as well as some variability in the size of the particles, were also observed in the two powdered reference samples (Figures S1 and S2, Supplementary Material).

3.2 HPLC-ESI-Q-ToF

The principal results obtained for samples NG and S64 have been described briefly previously in Martin de Fonjaudran *et al*. [3] and are integrated here with those obtained for samples BM and S63. HPLC-ESI-Q-ToF analysis revealed that the main organic components in all the samples were euxanthic acid (EA), euxanthone (E) and a sulphonate derivative of euxanthone (SE), as shown in Figure 6, where the Total Ion Chromatograms (TICs) of the BM reference sample and sample S63 are reported.

MS and MS/MS experiments, necessary to identify the molecules, were conducted using both negative and positive ionisation modes and the fragment ions present in the MS/MS spectra of E, EA and SE are reported in Table 2. The results obtained with negative ionisation on E and EA are in agreement with those obtained by Otlowska *et al.* [10]. SE was only detected in negative ionisation mode and details of its fragmentation are reported in Martin de Fonjaudran *et al*. [3]. In the positive ionisation mode, E and EA appeared to follow the same fragmentation pathways as in negative ionisation mode.

In addition, the chromatographic areas of E, EA and SE were integrated and their sum was calculated for all samples. The percentage ratios between the chromatographic areas of the three components and their sums were then considered (Table 2). Although these values are not quantitative concentrations, the results can still be used to compare relative amounts in the samples. Variations in the composition of Indian yellow, in terms of EA and E content, have been reported in the literature and linked to the quality of the pigment. The best quality is said to contain a high concentration of euxanthic acid, whereas cheaper grades contain elevated amounts of euxanthone [1, 42].

Analysis indeed revealed relative amounts of EA, E and SE varying from one sample to another. Sample S63 appeared more similar in composition to the NG reference, whereas sample S64 revealed a higher relative content of SE compared to the other samples.

Moreover, some minor components were detected only in sample S63 and were identified as four flavonoid molecules, *i.e.* morin, quercetin, luteolin and kaempferol (Figure 6, inset). In particular, morin and kaempferol were detected with both negative and positive ionisation modes, whereas quercetin and luteolin were only detected in the positive ionisation mode, due to their very low relative abundance and their slightly higher ionisation yield in positive mode. This result underlines the importance of running experiments in both ionisation modes whenever possible.

Morin and kaempferol are considered to be the main flavonoid components of cockspur thorn or kayu kuning (*Maclura cochinchinensis*), a plant whose native range extends from northern India and China, through Malaysia and Indonesia into Australia, and which has

been used since the 14th century in these parts of the world to produce a yellow dye [43]. It is reported that minor amounts of quercetin and luteolin can be present in the wood [44]. Therefore, the Indian yellow in sample S63 appears to be mixed with a yellow lake, probably obtained from kayu kuning extracts and used to create a slightly different yellow shade. To the best of our knowledge, this represents the first analytical evidence of such a mixture, although an account of traditional materials used in Mithila paintings (Bihar, northern India) reports the use of Indian yellow in combination with saffron (*Crocus sativus*) [45].

3.3 Photophysical properties

The photophysical properties of samples S63 and S64 were investigated in order to identify the key factors influencing their optical features (absorption and emission). The results were compared with those obtained for the reference samples (NG and BM), for which a study in aqueous solution was also possible.

Figure 7 reports the solid-state, normalised emission spectra for all the samples (λ_{ex} = 405 nm). Sample NG showed the highest red-shift emission (λ_{max} at 600 nm), while sample S63 showed the highest blue shift (λ_{max} = 570 nm). The λ_{max} of samples BM and S64 occur in between those of NG and S63.

The corresponding lifetime decays (Figure 7, inset) also showed different values. A mono-exponential decay was obtained for sample S63 (τ = 1.5 ns), whereas di-exponential curves were obtained for samples S64 (τ_1 = 0.5 ns, τ_2 = 1.5 ns), NG (τ_1 = 0.5 ns, τ_2 = 1.5 ns) and BM (τ_1 = 0.6 ns, τ_2 = 1.6 ns). A di-exponential decay generally suggests the presence of different packed domains, which can be driven by the π-π stacking and/or hydrogen bonds commonly occurring in solid-state organic samples [46]. The results show that this phenomenon occurred to some extent in all the samples except sample S63.

Different optical features were also found in the excitation spectra (closely related to the absorption spectra) of the NG and BM reference samples (Figure S3, Supplementary Material). The excitation spectra for S63 and S64 could not be measured, due to the small size of the samples. A spectral shift of *c.*20 nm was observed between the BM and NG samples. This was in agreement with the slight colour difference between the two samples, which was appreciable with a naked eye.

To confirm the presence of a di-exponential decay in the NG and BM reference samples, time-resolved measurements were acquired at different emission wavelengths (Figure 8). By measuring the decays at the rise, maximum and tail of the corresponding emission spectra, a progressive inversion of the relative weights between short and long lifetimes was observed (Table 3). This confirmed the presence of two different package domains mostly

emitting at the edges of the emission spectrum and being responsible for the optical output of the solid-state samples.

However, the differences observed in the optical features of the Indian yellow solid samples may also derive, in principle, from other factors, such as the different chemical composition, in terms of relative proportions of E, EA and SE (section 3.3), and the presence of impurities or additional components in the composition of the pigment (section 3.3).

In order to achieve a deeper understanding of these factors, a photophysical study in aqueous solution was performed for samples BM and NG. This allowed us to focus on the effect that a different chemical composition and/or the presence of impurities may have on the optical features, as packed domains do not form in solution. The experiments were not performed on samples S63 and S64 due to the small amount of material available.

Figure 9 shows that in both the excitation and emission spectra of sample BM a shoulder appears at longer wavelengths than in sample NG. In principle, this can be due to the slightly different chemical composition of the two samples, as shown by HPLC-ESI-Q-ToF analysis (section 3.3), or to the presence of inorganic impurities in sample BM [47], which are not present in the NG sample. Regardless of its origin, the shift observed between the spectra in the solid-state experiment (Figure 7) did not occur in solution (Figure 9).

This suggested that neither the different ratios between E, EA, SE (section 3.3) nor the presence of impurities are the driving forces for the spectral shift observed in the solid-state experiments. Otherwise, a shift should have been observed in both solution and solid-state conditions. Thus, it can reasonably be stated that the formation of different structural arrangements is the main cause for the spectral features/differences observed in the solid-state experiments [48].

Although this was proved for both reference samples, we cannot exclude the possibility that the presence of flavonoids might have influenced the shift observed for sample S63. Furthermore, the presence of impurities and/or differences in the relative abundance of various components in the pigment may be indirectly responsible for the different optical properties, as they may be among the driving forces for the formation of the solid-state structure during the preparation of the pigment.

3.4 TDDFT results

The emission spectra in water of the BM, NG, S63 and S64 samples were calculated and compared to the available experimental data in order to characterise the emission process and rationalise the difference observed at low energies for the BM and NG samples (see Figure 9). Two different models were implemented for the inclusion of the solvent with the polarisable conductor calculation model (CPCM): the linear response (LR-CPCM) and the

state specific (SS-CPCM), which consider the solvent in equilibrium with the excited state electron density by means of a self-consistent procedure. The vertical emission wavelengths obtained for the three dominant molecules present in the pigment samples (EA, SE and E) are presented in Table 4, together with their corresponding vertical absorption wavelengths calculated in our previous work [3]. The adiabatic and 0-0 transitions computed with the LR approximation, *i.e.* considering the initial and final states fully equilibrated with the solvent, are also reported. As indicated in section 2.6, the emission processes were considered as S_1-> S_0 transitions, where S_1 shows a $^1(\pi_H->\pi_L^*)$ character in water for all the three molecules under investigation, as shown earlier [3]. Vertical emissions for the optimised LR-CPCM and SS-CPCM curves emphasise the importance of solvent equilibration in solution: the SS-CPCM values are closer to those observed experimentally (see Figure 9).

The solvent reorganisation energies of the ground state evaluated by means of the SS-CPCM approach were 0.43 eV, 0.50 eV and 0.33 eV for EA, SE and E, showing a higher solvatochromic effect for euxhantone in a polar solvent. In all cases, the LR approach significantly overestimated the vertical emission process in solution, justifying the selection of advanced solvation models, as also indicated in the literature [49].

To characterise fully the emission process of the genuine pigment in water, we computed the vibrationally-resolved emission spectra of EA, SE and E by considering the emission as arising from the minima equilibrium solvated structures of the S_1 LR-CPMC curves.

Figure 10 presents the vibronic emission spectra of EA, SE and E calculated with the FC approximation as implemented in Gaussian09 providing the calculated state-specific emission energy as a vertical transition. The theoretical emission spectra for EA, SE and E were built up as a sum of 0-0 transitions and simultaneously excited vibrational contributions as derived from Gaussian09 and then convoluted with Gaussian functions, whose FWHMs were chosen to reproduce the final experimental spectra accurately.

The maximum peak in the calculated EA emission spectrum, around 456 nm, is mainly due to transitions of single and double simultaneously excited vibrational oscillators, while, in SE and E spectra, the maximum peaks, respectively at 466 and 446, are largely composed of only single vibrational transitions. In all the spectra, the tail at low energies is the result of higher order simultaneously vibrational transitions.

The spectrum of E showed the highest intensity and greatest blue-shift, as depicted in Figure 11a, this being the most solvated molecule in water. Figure 11b shows a comparison among the total emission spectra for BM (blue line), NG (green line), S63 (black line) and S64 (red line) samples calculated as a sum of the emission spectra of each molecule, scaled for their relative abundance (see Table 2 in section 3.3). Theoretical results were in excellent agreement with the available experimental data for the NG and BM reference compounds, showing a maximum peak in the emission spectra of all the pigment samples around 440 nm

and a more pronounced tail at low energies for the BM sample. The difference observed experimentally between NG and BM can be confidently ascribed to the relative composition of the two samples: the higher abundance of E in BM accounts for the higher tail in the spectrum. Based on the good agreement between calculated and experimental spectra of samples BM and NG, we can also assume that the spectra of samples S63 and S64 are accurately reproduced by theory, thus providing additional data that were impossible to obtain experimentally. In addition, no shift of the maximum was observed for these samples and only slight differences in the intensity of the tail were observed, echoing the behaviour of the reference samples and confirming the observations made above.

3.5 Py(HMDS)-GC-MS

Due to the absence of previous literature on the analysis of Indian yellow by Py-GC-MS, the NG reference sample was analysed to characterise the pigment, identify the main pyrolysis products and choose the optimum pyrolysis temperature. The pyrograms obtained at 400, 500 and 600°C showed two main pyrolysis products, namely the mono-trimethylsilyl derivatives of euxanthone and benzoic acid. The bis-trimethylsilyl derivative of euxanthone was also identified with low relative abundance. Figure 12a shows the pyrogram obtained for the NG reference sample at 500°C. The pyrograms obtained at 400 and 600°C are shown in the supplementary material (Figure S4, Supplementary Material).

In euxanthic acid, one of the hydroxyl groups of euxanthone is involved in the bond with the glucuronic acid. When thermal energy breaks this bond, the derivatisation of this position is unlikely to occur for kinetic and steric hindrance reasons, thus explaining the high relative abundance of mono-TMS euxanthone. Both mono-TMS and bis-TMS euxanthone can be considered as molecular markers for the presence of Indian yellow and their mass spectra are reported in Figure S5, Supplementary Material.

On the other hand, benzoic acid is a non-specific pyrolysis product easily formed during the pyrolysis of most phenolic molecules. In addition to these main pyrolysis products, some products derived from glucoronic acid were identified, such as 2-hydroxypropionic acid, 2-hydroxyacetic acid, hydroxylethylfuran, hydroxymethylcyclopentenone, hydroxypyranone, and other unidentified compounds. These pyrolysis products can also be considered non-specific, as they can easily derive from the pyrolysis of most sugars [50]. Some other non-specific pyrolysis products derived from euxanthone – phenol, benzenacetic acid, 4-hydroxybenzoic acid – were also present. A number of aliphatic monocarboxylic acids with chain lengths from seven to 18 carbon atoms were observed with relative low abundances, but their presence was due to instrumental contamination, as these compounds were also present in the analytical blanks.

When testing the optimum pyrolysis temperature, the results showed that the pyrolysis yield of euxanthone decreased as the temperature increased. On the other hand, the relative abundance of benzoic acid increased as the temperature increased, indicating that further decomposition of euxanthone to smaller non-specific molecules is favoured at higher temperatures. At 400°C, the highest relative abundance of euxanthone was obtained compared to benzoic acid. Nevertheless, we decided to use 500°C as the pyrolysis temperature for the wall painting samples, as the initial aim of Py(HMDS)-GC-MS analysis was to obtain some indication of the nature of the binding medium, and 400°C might have been too low to guarantee the pyrolysis of other materials. However, the relative decrease in the pyrolysis yield of euxanthone was acceptable at 500°C (Figure S4, Supplementary Material).

The results obtained for samples S63 and S64 generally showed a low relative abundance of pyrolysis products, as can be noticed by the lower signal/noise ratio compared to the reference sample (Figure 12b and 12c). Mono-TMS euxanthone was clearly detected in both samples, proving the technique to be suitable for the identification of Indian yellow in historic samples. Unfortunately, the results did not allow unequivocal identification of the binding medium. Although the detection of aliphatic carboxylic acids, such as palmitic and stearic acids, as the main pyrolysis products could indicate the presence of a lipid material in the samples [51], contamination is also possible, as these carboxylic acids were also present in the analytical blank. The presence of glycerol alongside the carboxylic acids in the pyrogram obtained for sample S63 is a stronger clue to the presence of a triglyceride, but not enough to confirm the presence of oil. Azelaic acid, usually formed by semi-drying or drying oils, was not detected in the samples. The presence of an oil binder may be therefore considered but the amount of sample did not allow for further analysis to confirm this hypothesis. However, the presence of a small amount of binder should not significantly influence the photophysical properties of Indian yellow. In fact, emission from a binder would normally fall at lower wavelengths [52]. While this would shift the colour of the images towards the blue, it would easily be picked up by spectroscopy as a separate emission. Nevertheless, a comprehensive study of the photoluminescence of Indian yellow mixed with different binding media would represent an interesting topic for future research.

4. Conclusions

This work presents an in-depth investigation of two reference and two historical samples (early 17th-century wall painting in the Garh Palace, Bundi, India) containing Indian yellow. The main aim was to identify factors responsible for differences in optical properties, and

provide new insights into the photophysical properties of this relatively poorly-studied pigment.

The paint layer in the two historic samples appeared different in terms of the distribution, size and colour of the pigment particles, although this did not seem to correspond to any specific elemental difference. All the samples analysed showed slight differences in their chemical composition, mainly related to the relative amounts of EA, E and SE. Only sample S63, the lightest in colour, revealed the presence of additional flavonoids, which are likely to derive from the plant cockspur thorn or kayu kuning (*Maclura cochinchinensis*).

The photophysical properties of the samples also showed differences. Solid-state experiments revealed a shift of the maximum in the emission spectra and di-exponential lifetime decays for all the samples except S63. However, experiments in solution did not highlight any shift, suggesting that this is mainly produced by different structural arrangements occurring in the solid state and probably driven by π-π stacking and/or hydrogen bonds. Despite the absence of a shift in the spectra acquired in water, a difference in intensity was observed at low energies. This was ascribed to the different chemical composition of the samples in terms of relative amounts of EA, E and SE by using TDDFT calculations, which also allowed the simulation of the spectra acquired in water for the historic samples. Although conclusive indications of the binding medium were not obtained by Py(HMDS)-GC-MS, Indian yellow was characterised with this technique for the first time and euxanthone was proved to be a valuable biomarker for the identification of the pigment. Finally, this study highlighted the refined and complex use of this pigment by artists producing monumental paintings in Rajasthan in the 17th century. Different yellow hues were achieved through subtle combination of Indian yellow and yellow organic colourants, as well as different underlying preparation layers.

This information on the pigment composition, mixtures and layering of materials is extremely important for conservators as they address the preservation and treatment of these culturally significant artefacts; it provides a basis not only to understand colour variations for this particular pigment, but also to monitor possible colour changes through time, whether due to environmental parameters or exposure to conservation materials, and therefore to design and implement informed and safer conservation interventions.

Acknowledgements

This work was generously funded by a Leverhulme Trust Research Project Grant (LuminArt Project; grant number: RPG-2012-704). The conservation programme of the Bundi wall paintings, led by the Conservation of Wall Painting Department of the Courtauld Institute of Art in collaboration with the Kudevi Ashapura Mataji Trust, is sponsored by AkzoNobel within a collaborative programme with the Leon Levy Foundation Centre for Conservation Studies

at Nagaur. We wish to thank Professor David Park for his support with the wall painting conservation project and research and Caroline Cartwright at the British Museum (Scientific Department) for her support and useful discussions. The reference sample of Indian yellow was kindly provided by Marika Spring at the National Gallery in London. Gianluca Accorsi wishes to thank the project MAAT (MIUR- PON02_00563_3316357 – CUP B31C12001230005). As an Andrew W. Mellon Postdoctoral Research Fellow, Diego Tamburini would like to thank the Andrew W. Mellon foundation.

References

[1] N.S. Baer, A. Joel, R.L. Feller, N. Indictor, Indian yellow, in: R.L. Feller (Ed.) Artists' pigments: a handbook of their history and characteristics, Archetype Publications, London, 1986, pp. 17-36.
[2] N. Eastaugh, V. Walsh, T. Chaplin, R. Siddall, Pigment compendium: a dictionary and optical microscopy of historical pigments. , Butterworth-Heinemann, 2008.
[3] C. Martin de Fonjaudran, A. Acocella, G. Accorsi, D. Tamburini, G. Verri, A. Rava, S. Whittaker, F. Zerbetto, D. Saunders, Optical and theoretical investigation of Indian yellow (euxanthic acid and euxanthone), Dyes and Pigments, 144 (2017) 234-241.
[4] M.C. Beach, Bundi Fort : a Rajput world., The Marg Foundation, Mumbai, India, 2016.
[5] T.R. Ravindran, A.K. Arora, S. Ramya, R.V. Subba Rao, B. Raj, Raman spectroscopic study of medieval Indian art of 17th century, Journal of Raman Spectroscopy, 42 (2011) 803-807.
[6] I. Reiche, R. Britzke, G. Bukalis, U. Reinholz, H.P. Weise, R.D. Gadebusch, An external PIXE study: Mughal painting pigments, X-Ray Spectrometry, 34 (2005) 42-45.
[7] R. Ploeger, A. Shugar, The story of Indian yellow – excreting a solution, Journal of Cultural Heritage, 24 (2017) 197-205.
[8] T.N. Mukharji, Piuri or Indian yellow in, Journal of the Society of the Arts, 32 (1883-84) 16-17.
[9] D.L.A. de Faria, H.G.M. Edwards, V. Careaga, N. Walt, M.S. Maier, A definitive analytical spectroscopic study of Indian yellow, an ancient pigment used for dating purposes, Forensic Science International, 271 (2017) 1-7.
[10] O. Otlowska, M. Slebioda, M. Wachowiak, M. Sliwka-Kaszynska, Identification and characterization of the Indian Yellow dyestuff and its degradation products in historical oil paint tube by liquid chromatography mass spectrometry, RSC Advances, 5 (2015) 48786-48792.
[11] G.D. Smith, Cow urine, Indian yellow, and art forgeries: An update, Forensic Science International, 276 (2017) e30-e34.
[12] E. Isacco, J. Darrah, The Ultraviolet-Infrared method of analysis, a scientific approach to the study of indian miniatures, Artibus Asiae, 53 (1993) 470-491.
[13] J.H. Townsend, The materials of J.M.W. Turner: pigments, Studies in Conservation, 38 (1993) 231-254.
[14] K. Janssens, G. Van der Snickt, F. Vanmeert, S. Legrand, G. Nuyts, M. Alfeld, L. Monico, W. Anaf, W. De Nolf, M. Vermeulen, J. Verbeeck, K. De Wael, Non-Invasive and Non-Destructive Examination of Artistic Pigments, Paints, and Paintings by Means of X-Ray Methods, Topics in Current Chemistry, 374 (2016) 81.
[15] M. Manfredi, E. Barberis, A. Rava, E. Robotti, F. Gosetti, E. Marengo, Portable diffuse reflectance infrared Fourier transform (DRIFT) technique for the non-invasive identification of canvas ground: IR spectra reference collection, Analytical Methods, 7 (2015) 2313-2322.

598 [16] B. Brunetti, C. Miliani, F. Rosi, B. Doherty, L. Monico, A. Romani, A. Sgamellotti, Non-
599 invasive Investigations of Paintings by Portable Instrumentation: The MOLAB Experience,
600 Topics in Current Chemistry, 374 (2016) 10.
601 [17] A. Cosentino, Identification of pigments by multispectral imaging; a flowchart method,
602 Heritage Science, 2 (2014) 8.
603 [18] G. Verri, The spatially resolved characterisation of Egyptian blue, Han blue and Han
604 purple by photo-induced luminescence digital imaging, Analytical and Bioanalytical
605 Chemistry, 394 (2009) 1011-1021.
606 [19] G. Accorsi, G. Verri, A. Acocella, F. Zerbetto, G. Lerario, G. Gigli, D. Saunders, R.
607 Billinge, Imaging, photophysical properties and DFT calculations of manganese blue (barium
608 manganate(vi) sulphate) - a modern pigment, Chemical Communications, 50 (2014) 15297-
609 15300.
610 [20] J. Dyer, S. Sotiropoulou, A technical step forward in the integration of visible-induced
611 luminescence imaging methods for the study of ancient polychromy, Heritage Science, 5
612 (2017) 24.
613 [21] K. Keune, A. van Loon, J.J. Boon, SEM Backscattered-Electron Images of Paint Cross
614 Sections as Information Source for the Presence of the Lead White Pigment and Lead-
615 Related Degradation and Migration Phenomena in Oil Paintings, Microscopy and
616 Microanalysis, 17 (2011) 696-701.
617 [22] C. Higgitt, M. Spring, D. Saunders, Pigment-medium Interactions in Oil Paint Films
618 containing Red Lead or Lead-tin Yellow, National Gallery Technical Bulletin, 24 (2003) 75–
619 95.
620 [23] M.P. Colombini, F. Modugno, Organic Materials in Art and Archaeology, Organic Mass
621 Spectrometry in Art and Archaeology, John Wiley & Sons, Ltd, 2009, pp. 1-36.
622 [24] G. Accorsi, G. Verri, M. Bolognesi, N. Armaroli, C. Clementi, C. Miliani, A. Romani, The
623 exceptional near-infrared luminescence properties of cuprorivaite (Egyptian blue), Chemical
624 Communications, (2009) 3392-3394.
625 [25] D. Comelli, V. Capogrosso, C. Orsenigo, A. Nevin, Dual wavelength excitation for the
626 time-resolved photoluminescence imaging of painted ancient Egyptian objects, Heritage
627 Science, 4 (2016) 21.
628 [26] C. Clementi, F. Rosi, A. Romani, R. Vivani, B.G. Brunetti, C. Miliani, Photoluminescence
629 Properties of Zinc Oxide in Paints: A Study of the Effect of Self-Absorption and Passivation,
630 Applied Spectroscopy, 66 (2012) 1233-1241.
631 [27] G. Verri, D. Saunders, Xenon flash for reflectance and luminescence (multispectral)
632 imaging in cultural heritage applications, The British Museum Technical Bulletin, 8 (2014).
633 [28] J. Dyer, G. Verri, J. Cupitt, Multispectral imaging in reflectance and photo-induced
634 luminescence modes: a user manual, 2013.
635 [29] P. Hohenberg, W. Kohn, Inhomogeneous Electron Gas, Physical Review, 136 (1964)
636 B864-B871.
637 [30] R.E. Stratmann, G.E. Scuseria, M.J. Frisch, An efficient implementation of time-
638 dependent density-functional theory for the calculation of excitation energies of large
639 molecules, The Journal of Chemical Physics, 109 (1998) 8218-8224.
640 [31] R. Bauernschmitt, R. Ahlrichs, Treatment of electronic excitations within the adiabatic
641 approximation of time dependent density functional theory, Chemical Physics Letters, 256
642 (1996) 454-464.
643 [32] M.E. Casida, C. Jamorski, K.C. Casida, D.R. Salahub, Molecular excitation energies to
644 high-lying bound states from time-dependent density-functional response theory:
645 Characterization and correction of the time-dependent local density approximation ionization
646 threshold, The Journal of Chemical Physics, 108 (1998) 4439-4449.
647 [33] M. Frisch, G. Trucks, H.B. Schlegel, G. Scuseria, M. Robb, J. Cheeseman, G. Scalmani,
648 V. Barone, B. Mennucci, G. Petersson, Gaussian 09, revision D. 01, Gaussian, Inc.,
649 Wallingford CT, 2009.
650 [34] A.D. Becke, Density-functional thermochemistry. III. The role of exact exchange, The
651 Journal of Chemical Physics, 98 (1993) 5648-5652.

[35] V. Barone, M. Cossi, Quantum Calculation of Molecular Energies and Energy Gradients in Solution by a Conductor Solvent Model, The Journal of Physical Chemistry A, 102 (1998) 1995-2001.
[36] M. Cossi, N. Rega, G. Scalmani, V. Barone, Energies, structures, and electronic properties of molecules in solution with the C-PCM solvation model, Journal of Computational Chemistry, 24 (2003) 669-681.
[37] D.R. Lide, CRC handbook of chemistry and physics, CRC Press, Boca Raton, 2005.
[38] M. Cossi, V. Barone, Time-dependent density functional theory for molecules in liquid solutions, The Journal of Chemical Physics, 115 (2001) 4708-4717.
[39] R. Cammi, B. Mennucci, Linear response theory for the polarizable continuum model, The Journal of Chemical Physics, 110 (1999) 9877-9886.
[40] R. Improta, G. Scalmani, M.J. Frisch, V. Barone, Toward effective and reliable fluorescence energies in solution by a new state specific polarizable continuum model time dependent density functional theory approach, The Journal of Chemical Physics, 127 (2007) 074504.
[41] R. Improta, V. Barone, G. Scalmani, M.J. Frisch, A state-specific polarizable continuum model time dependent density functional theory method for excited state calculations in solution, The Journal of Chemical Physics, 125 (2006) 054103.
[42] R.B.G. Kew, Indian Yellow, Bulletin of Miscellaneous Information, 39 (1890) 45-50.
[43] D. Cardon, Natural Dyes. Sources, Tradition, Technology and Science, Archetype Publications Ltd., London, 2007.
[44] D. Richardson, S. Richardson, Asian textiles studies, 2017.
[45] V. Jha, Indigenous colours in Mithila (north Bihar): a historical perspective, Indian Journal of History and Science 37 (2002) 37-55.
[46] A.K. Srivastava, A. Singh, L. Mishra, Tuning of Aggregation Enhanced Emission and Solid State Emission from 1,8-Naphthalimide Derivatives: Nanoaggregates, Spectra, and DFT Calculations, The Journal of Physical Chemistry A, 120 (2016) 4490-4504.
[47] S. Hofener, P.C. Kooijman, J. Groen, F. Ariese, L. Visscher, Fluorescence behavior of (selected) flavonols: a combined experimental and computational study, Physical Chemistry Chemical Physics, 15 (2013) 12572-12581.
[48] S.-L. Zheng, P. Coppens, Syntheses, Structures, Photoluminescence and Theoretical Studies of Xanthone in Crystalline Resorcinarene-Based Inclusion Complexes, Chemistry – A European Journal, 11 (2005) 3583-3590.
[49] D. Jacquemin, A. Planchat, C. Adamo, B. Mennucci, TD-DFT Assessment of Functionals for Optical 0–0 Transitions in Solvated Dyes, Journal of Chemical Theory and Computation, 8 (2012) 2359-2372.
[50] D. Fabbri, G. Chiavari, Analytical pyrolysis of carbohydrates in the presence of hexamethyldisilazane, Analytica Chimica Acta, 449 (2001) 271-280.
[51] I. Bonaduce, A. Andreotti, Py-GC/MS of Organic Paint Binders, Organic Mass Spectrometry in Art and Archaeology, John Wiley & Sons, Ltd, 2009, pp. 303-326.
[52] G. Verri, A. Keller, F. Piqué, A. Aldrovandi, Ultraviolet-induced luminescence imaging, in: F. Piqué, G. Verri (Eds.) Organic Materials in Wall Paintings, The Getty Conservation Institute, Los Angeles, 2015, pp. 76-82.

Figure 1. South wall of the Badal Mahal depicting rulers of Bundi with Hindu deities (left). Detail of a hunting scene on the west wall of the Badal Mahal (right). The painting from which the samples were taken is shown in [3] and some details are present in Figure 2.

Figure 2. Detailed views of the south wall of the Badal Mahal showing the location of sample S63 (left) and sample (S64) right. The overall view of the south wall is presented in Martin de Fonjaudran *et al*. [3].

Figure 3. Top: luminescence images of the area from which sample S64 was taken (visible image [left)], UV-VISL [middle] and UV-IRL [right]). In-situ observation of PL properties of sample S63 location showed similar characteristics to the brighter yellow observed in the above images. Bottom: visible, UV-VISL, UV-IRL and VIS-IRL luminescence images of BM (top) and NG (bottom) reference samples – see Table 1 for details of imaging conditions

Figure 4. Images obtained by optical microscopy under UV illumination (top) and scanning electron microscopy in BSE mode (bottom) corresponding to the same region of the cross-sections for samples **a)** S63 and **b)** S64.

Figure 5. EDS maps obtained for an area of the cross-sections of samples a) S63 and b) S64.

Figure 6. Total Ion Chromatograms obtained by HPLC-ESI-Q-ToF analysis of **a)** BM reference and **b)** S63, showing euxanthone (E), euxanthic acid (EA) and euxanthone sulphonate (SE) as the main components. Inset: Extract Ion Chromatograms showing the flavonoids detected in sample S63. * = background peak.

Figure 7. Main window: Corrected normalised emission spectra of samples NG (olive), S64 (red), BM (blue) and S63 (black) excited at 405 nm. Inset: Corresponding lifetime decays, λ_{em} = 600 nm.

Figure 8. Lifetime decays (λ_{exc} = 405 nm) of samples BM (upper, blue) and NG (lower, olive) acquired at 530, 560 and 650 nm, corresponding to the rise, maximum and tail of the emission spectra.

Figure 9. Corrected excitation (left, λ_{em} = 600 nm) and emission (right, λ_{exc} = 405 nm) spectra of NG (olive) and BM (blue) in aqueous solution. Inset (right window): Corresponding lifetime decays (λ_{exc} = 405 nm).

Figure 10. Emission spectra computed in water (black solid line) of **a)** EA, **b)** SE and **c)** E molecules and decomposition of the spectra into contributions from the 0-0 transition (0) and the n (n=1,4) simultaneously excited oscillators.

Figure 11. a) Emission spectra calculated in water for E (red line), EA (green line) and SE (blue line); **b)** Emission spectra calculated in water for BM (blue line) and NG (green line) S63 (black line) and S64 (red line) samples.

Figure 12. Total Ion Chromatograms (TICs) obtained by Py(HMD)-GC-MS analysis of a) the NG reference sample of Indian yellow, **b)** S63 and **c)** S64. Pyrolysis temperature: 500°C

747

748 **Table 1.** Band pass filters and related spectral ranges for PL imaging of reference samples

Imaging	Excitation filters	Excitation spectral range	Emission filter	Emission spectral range
UV-VISL	Xnite 330C + Xnite CC1	*c.* 280-390 nm	Schott KV418 + IDAS UIBAR	*c.*400-700 nm
UV-IRL1	Xnite 330C + Xnite CC1	*c.* 280-390 nm	Xnite 715	715-1100 nm
UV-IRL2	Xnite 330C + Xnite CC1	*c.* 280-390 nm	Xnite 830	830-1100 nm
VIS-IRL1	BP450 + Xnite CC1	*c.* 420-480 nm	Xnite 715	715-1100 nm
VIS-IRL2	BP525 + Xnite CC1	*c.* 490-560 nm	Xnite 715	715-1100 nm
VIS-IRL3	BP625 + Xnite CC1	*c.* 590-680 nm	Xnite 715	715-1100 nm

749

750

751

752 **Table 2.** Mass spectrometry data obtained with positive and negative ionisation modes and
753 percentage areas calculated for Indian yellow components euxanthone (E), euxanthic acid
754 (EA) and euxanthone sulphonate (SE). Standard deviations refer to triplicates.

		$[M]^-$	**$[M]^+$**	**Positive fragment ions**	**Negative fragment ions**	**$A\%_{BM\ ref}$**	**$A\%_{NG\ ref}$**	**$A\%_{S63}$**	**$A\%_{S64}$**
E	$C_{13}H_8O_4$	227.0350	229.0495	211, 201, 183, 173, 155, 127,	199, 181, 171, 155, 143, 117, 91, 79	21.5 ± 0.3	7.9 ± 0.2	3.6 ± 0.1	5.6 ± 0.1
EA	$C_{19}H_{16}O_{10}$	403.0671	405.0816	229, 201, 141, 113, 85	227, 199, 171, 113, 85	71.3 ± 0.2	77.4 ± 0.8	81.5 ± 0.2	65.4 ± 0.4
SE	$C_{13}H_8O_7S$	306.9918	ND*	ND*	227, 199, 171, 143, 117	7.3 ± 0.2	14.7 ± 0.6	14.9 ± 0.1	28.9 ± 0.4

755 * ND = not detected

756

757

758 **Table 3.** Lifetime decays and relative weights (%) of BM and NG acquired at different
759 wavelengths.

	λ_{em} = 530 nm	λ_{em} = 560 nm	λ_{em} = 650 nm
BM	τ_1 = 0.6 ns (18%) τ_2 = 1.6 ns (82%)	τ_1 = 0.6 ns (49%) τ_2 = 1.6 ns (51%)	τ_1 = 0.6 ns (74%) τ_2 = 1.6 ns (27%)
NG	τ_1 = 0.5 ns (53%) τ_2 = 1.5 ns (47%)	τ_1 = 0.5 ns (87%) τ_2 = 1.5 ns (13%)	τ_1 = 0.5 ns (94%) τ_2 = 1.5 ns (6%)

760

761

762

763 **Table 4.** Calculated vertical absorption energies (ΔE_{Abs}), vertical emission energies in LR
764 approximation ($\Delta E_{Em}^{(LR)}$), vertical emission energies in SS approximation ($\Delta E_{Em}^{(SS)}$), adiabatic
765 ($\Delta E_{Em}^{(ad)\text{-}LR}$) and 0-0 ($\Delta E_{Em}^{0\text{-}0\text{-}LR}$) transition energies in water at the B3LYP/TZVP level of
766 theory for EA, SE and E compounds. All energies are reported in eV (nm).

	ΔE_{Abs}[a]	$\Delta E_{Em}^{(LR)}$	$\Delta E_{Em}^{(SS)}$	$\Delta E_{Em}^{(ad)\text{-}LR}$	$\Delta E_{Em}^{0\text{-}0\text{-}LR}$
EA	3.41 (363)	2.98 (416)	2.71 (456)	3.14 (394)	3.03 (408)
SE	3.45 (359)	2.94 (421)	2.66 (466)	3.15 (393)	3.06 (404)
E	3.44 (360)	2.94 (421)	2.77 (446)	3.11 (398)	3.00 (412)

767 [a] as described in [3]


S63
1 cm

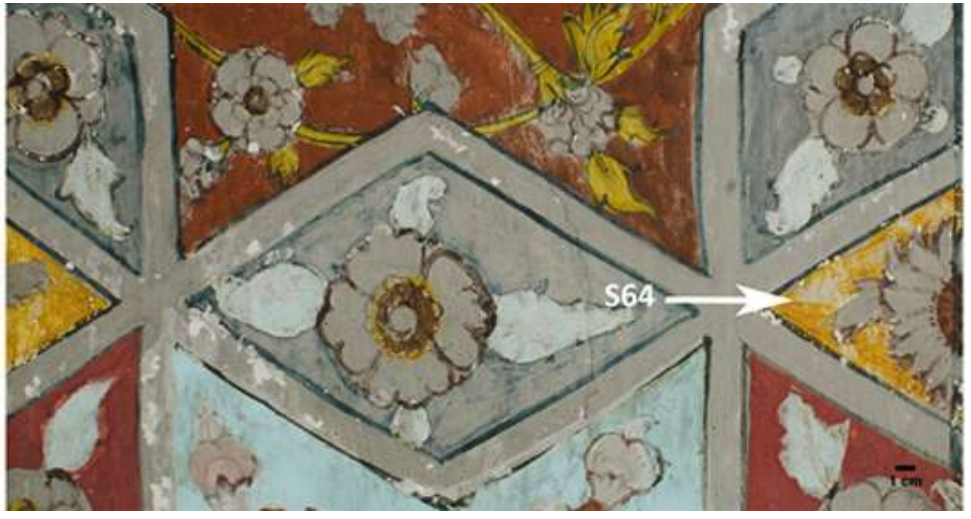
S64
1 cm

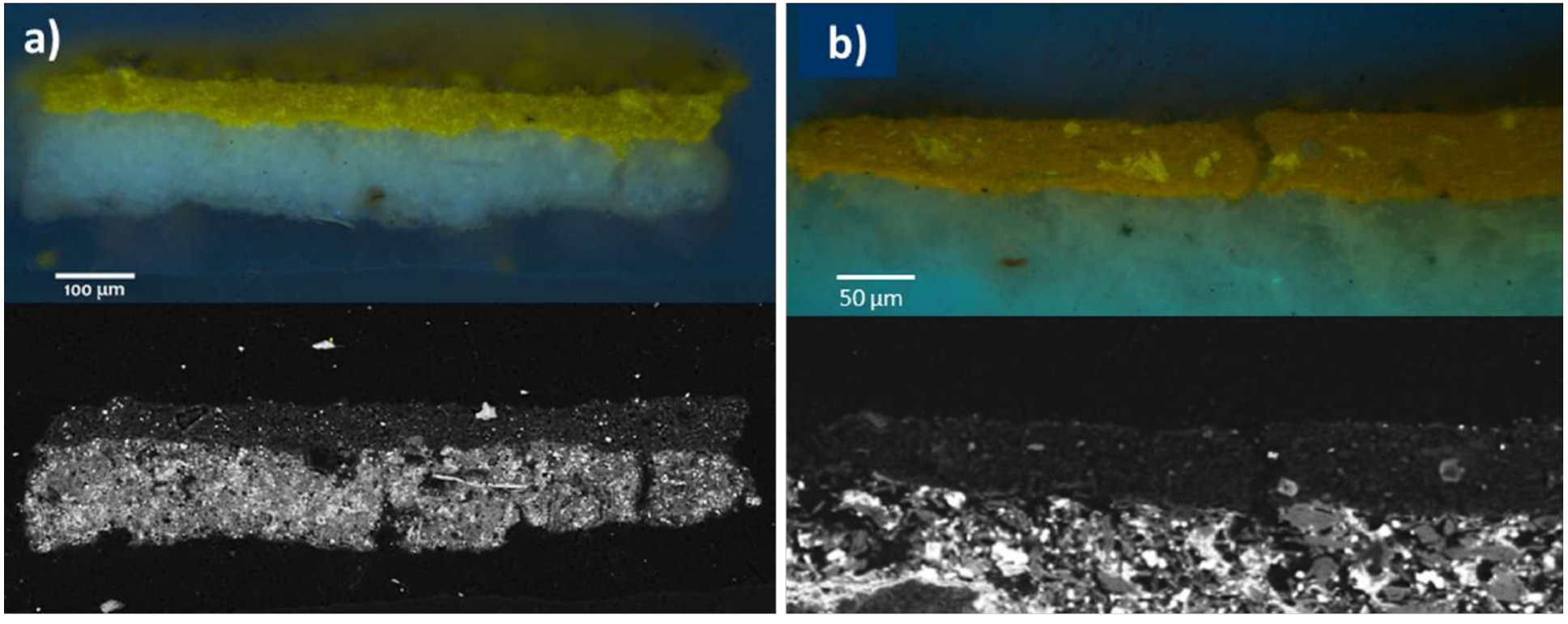
a)
100 µm
b)
50 µm

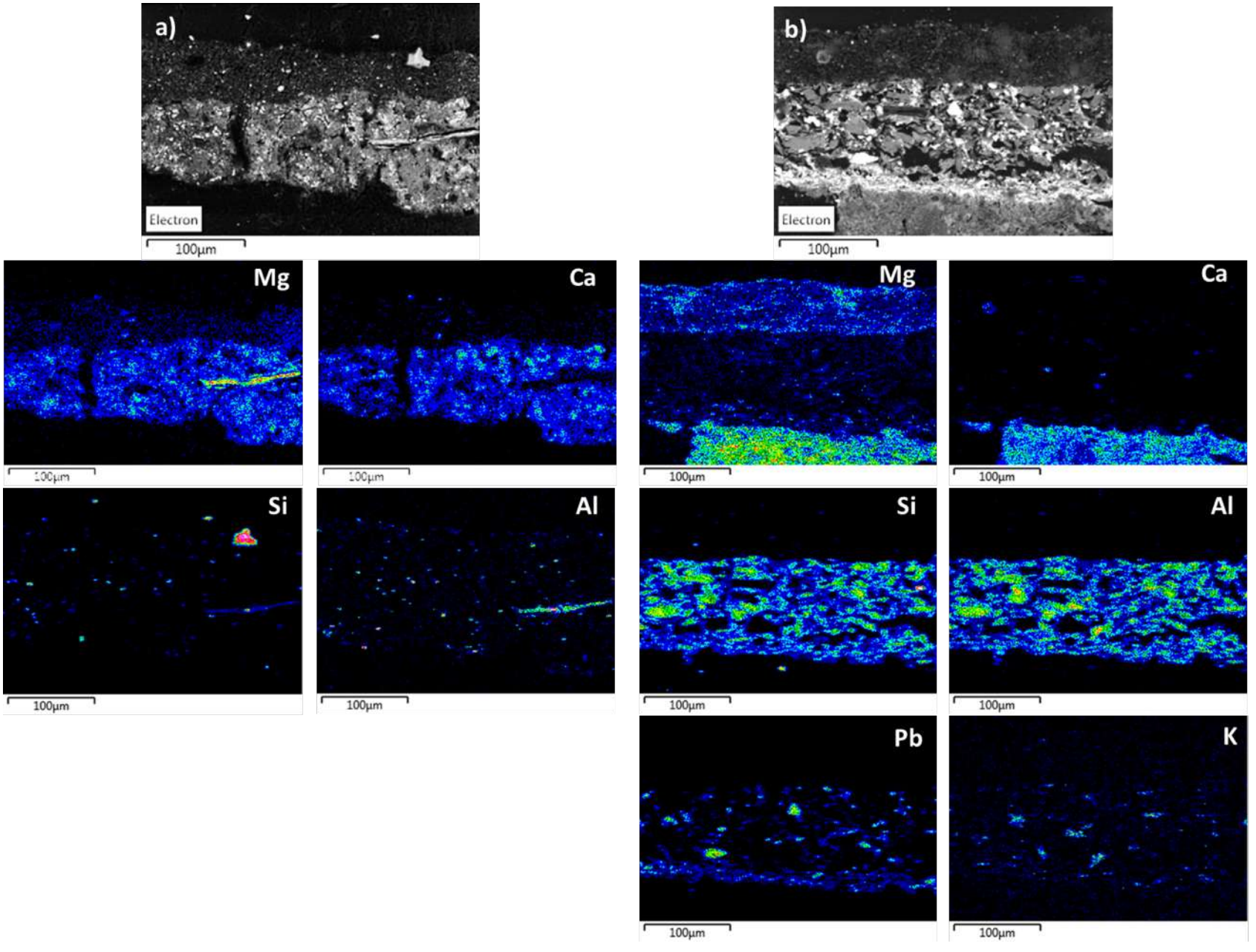
a)
Electron
100µm
b)
Electron
100µm
Mg
100µm
Ca
100µm
Mg
100µm
Ca
100µm
Si
100µm
Al
100µm
Si
100µm
Al
100µm
Pb
100µm
K
100µm

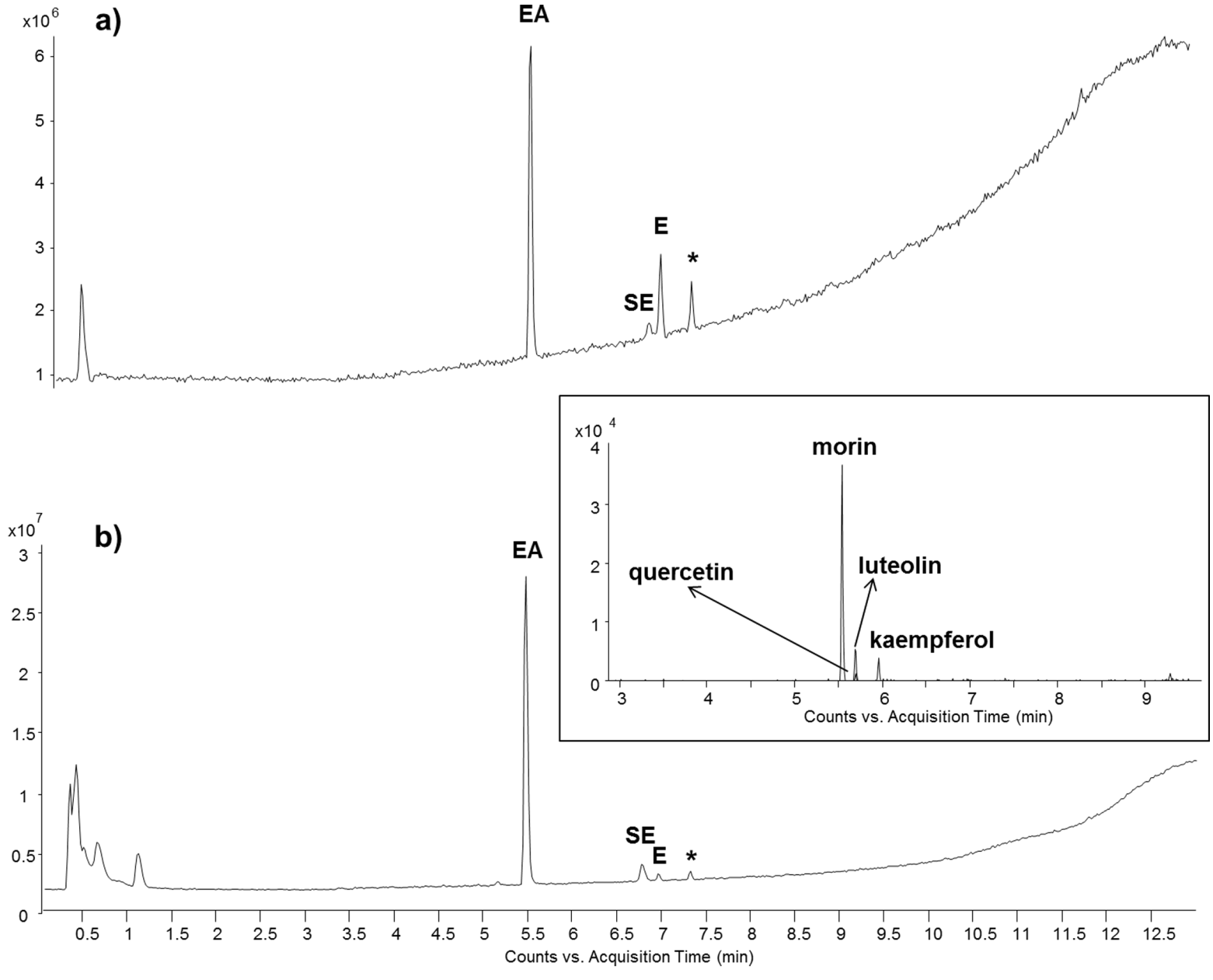
a)
x10 6
6
5
4
3
2
1
EA
E
*
SE
b)
x10 7
3
2.5
2
1.5
1
0.5
0
EA
SE
E
*
0.5 1 1.5 2 2.5 3 3.5 4 4.5 5 5.5 6 6.5 7 7.5 8 8.5 9 9.5 10 10.5 11 11.5 12 12.5
Counts vs. Acquisition Time (min)
x10 4
4
3
2
1
0
morin
quercetin
luteolin
kaempferol
3 4 5 6 7 8 9
Counts vs. Acquisition Time (min)

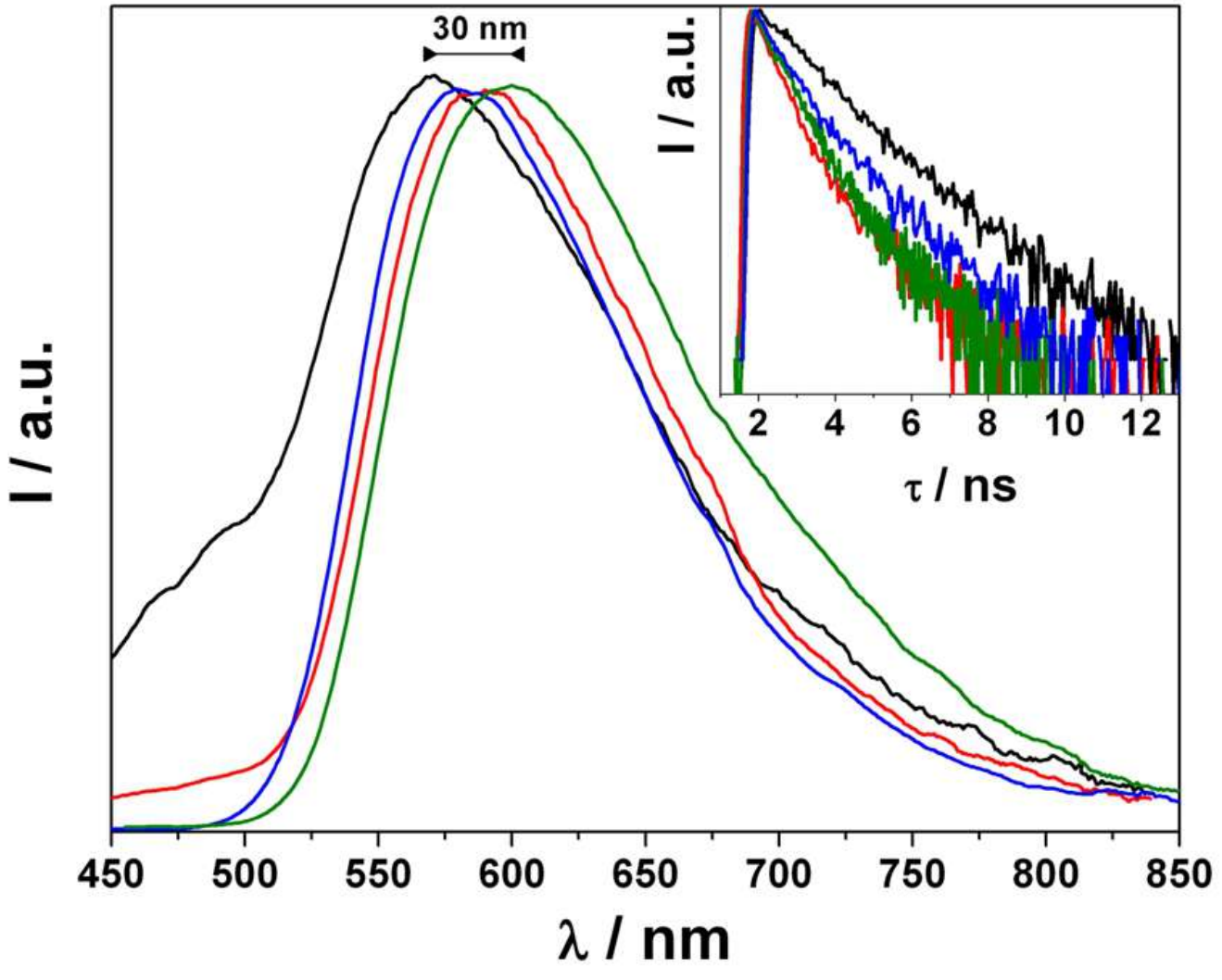
30 nm
I / a.u.
450
500
550
600
650
700
750
800
850
λ / nm
I / a.u.
2
4
6
8
10
12
τ / ns

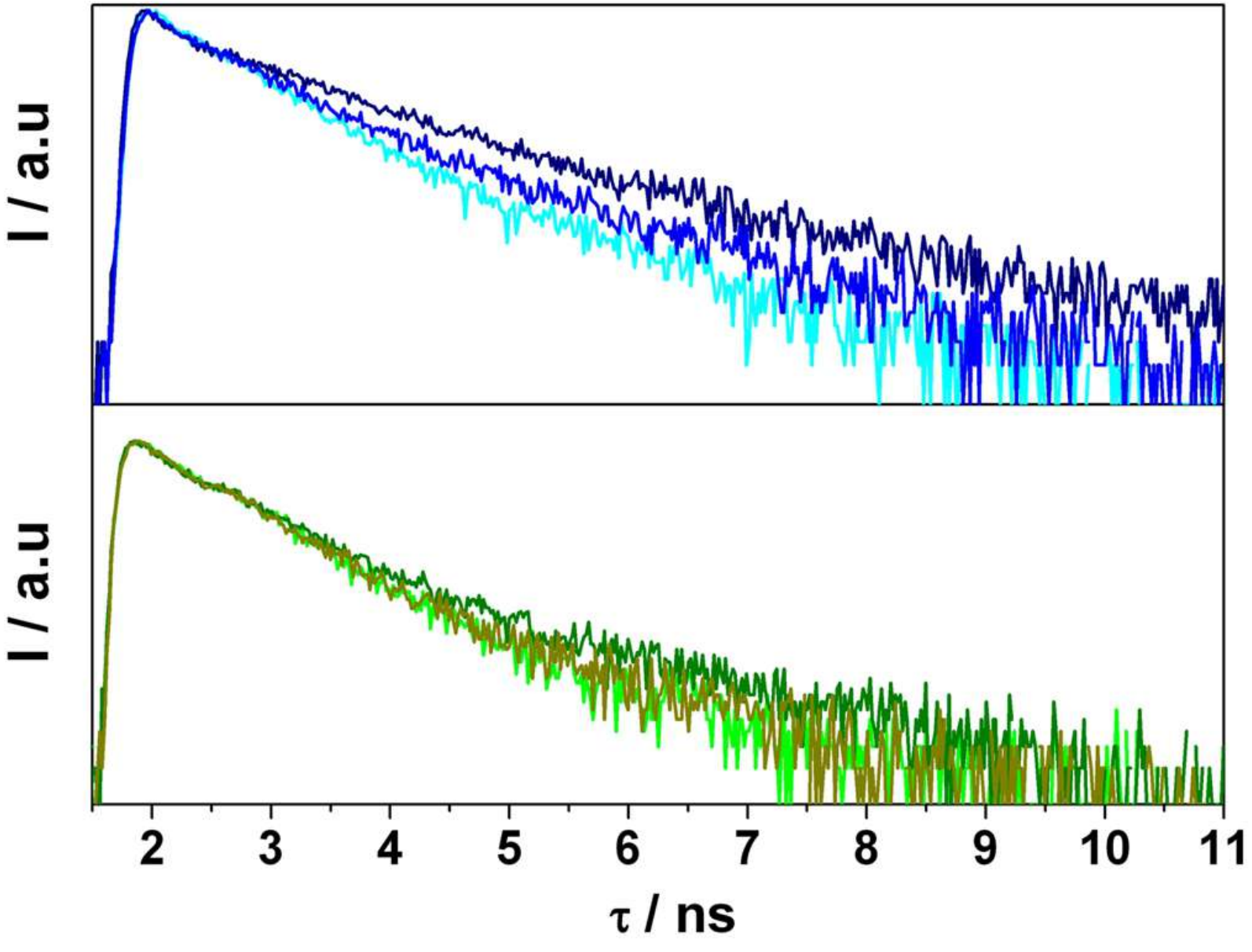
I / a.u
I / a.u
2
3
4
5
6
7
8
9
10
11
τ / ns

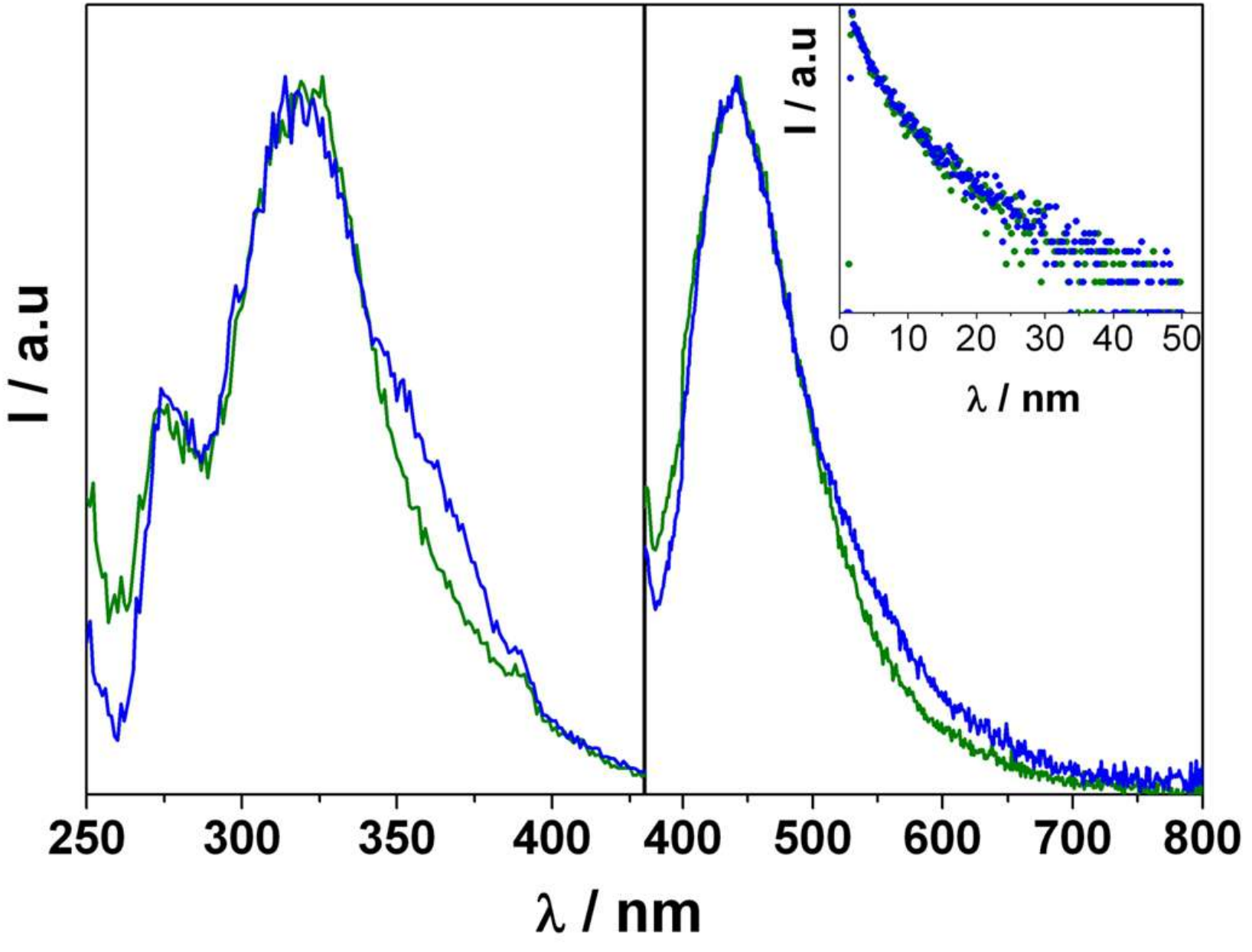
I / a.u
250
300
350
400
400
500
600
700
800
λ / nm
I / a.u
0
10
20
30
40
50
λ / nm

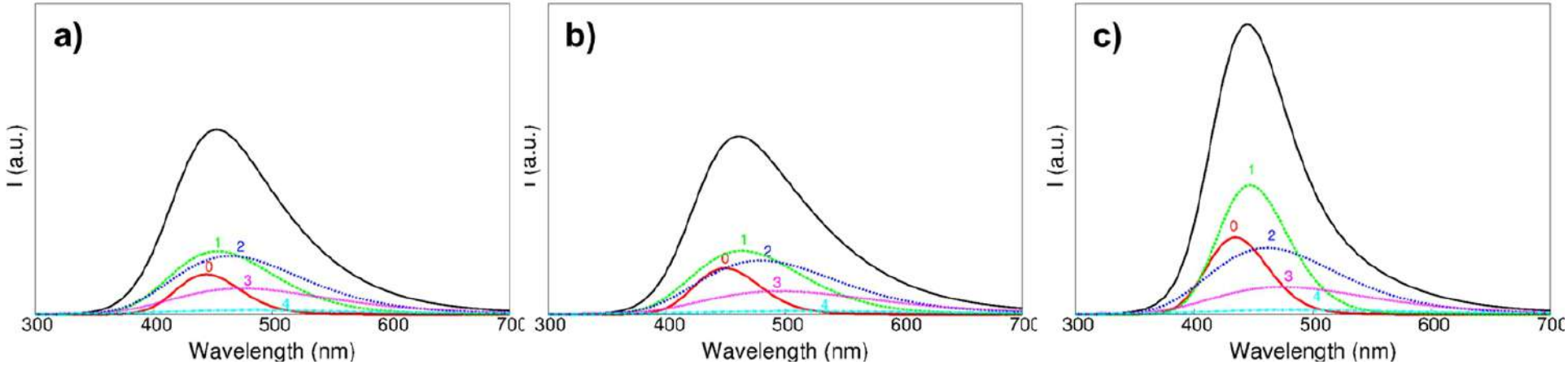
a)
b)
c)
I (a.u.)
Wavelength (nm)
300
400
500
600
700
0
1
2
3
4

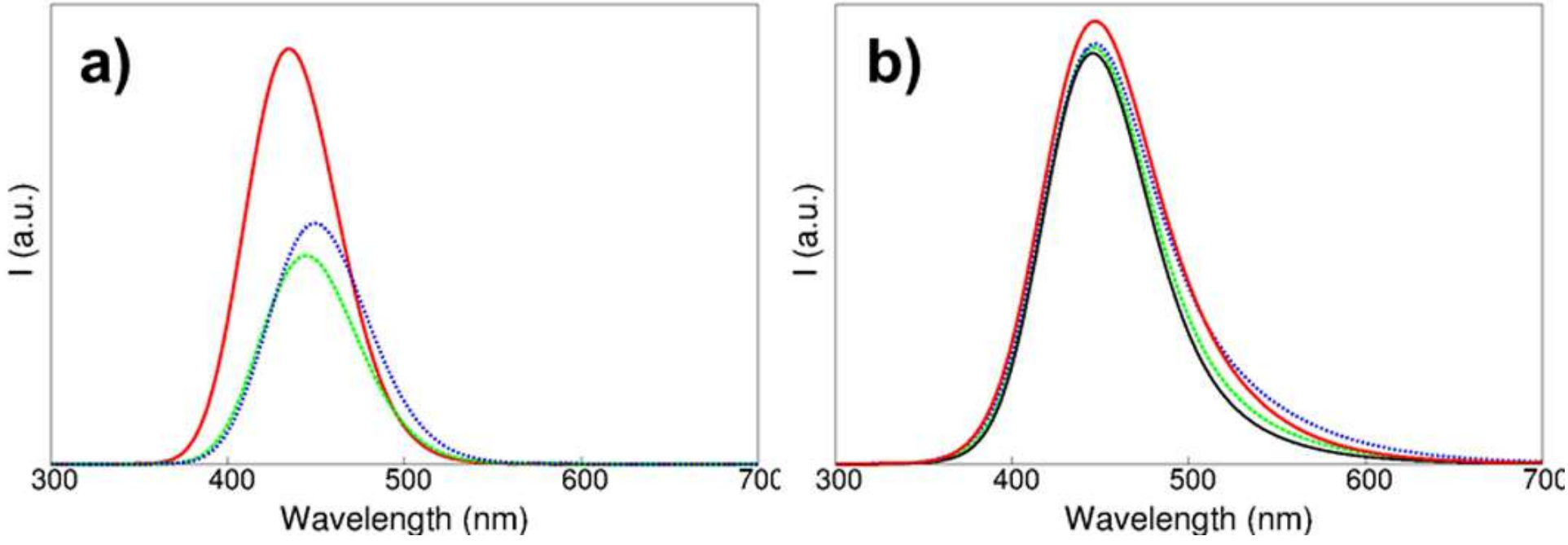
a)
I (a.u.)
300
400
500
600
700
Wavelength (nm)
b)
I (a.u.)
300
400
500
600
700
Wavelength (nm)

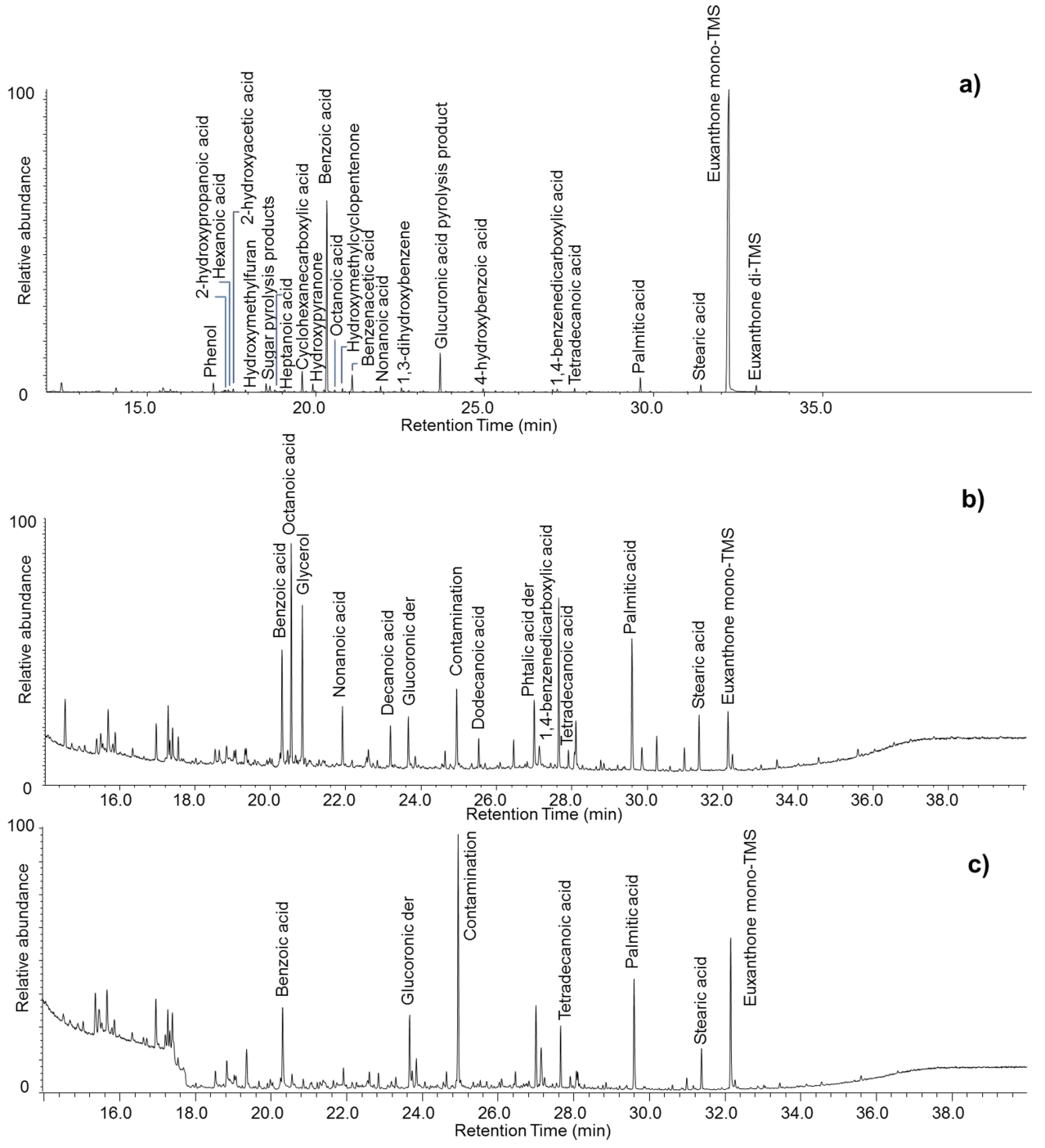
a)
Relative abundance
100
0
Phenol
2-hydroxypropanoic acid
Hexanoic acid
Hydroxymethylfuran
2-hydroxyacetic acid
Sugar pyrolysis products
Heptanoic acid
Cyclohexanecarboxylic acid
Hydroxypyranone
Benzoic acid
Octanoic acid
Hydroxymethylcyclopentenone
Benzenacetic acid
Nonanoic acid
1,3-dihydroxybenzene
Glucuronic acid pyrolysis product
4-hydroxybenzoic acid
1,4-benzenedicarboxylic acid
Tetradecanoic acid
Palmitic acid
Stearic acid
Euxanthone mono-TMS
Euxanthone di-TMS
15.0
20.0
25.0
30.0
35.0
Retention Time (min)
b)
Relative abundance
100
0
Benzoic acid
Octanoic acid
Glycerol
Nonanoic acid
Decanoic acid
Glucoronic der
Contamination
Dodecanoic acid
Phtalic acid der
1,4-benzenedicarboxylic acid
Tetradecanoic acid
Palmitic acid
Stearic acid
Euxanthone mono-TMS
16.0
18.0
20.0
22.0
24.0
26.0
28.0
30.0
32.0
34.0
36.0
38.0
Retention Time (min)
c)
Relative abundance
100
0
Benzoic acid
Glucoronic der
Contamination
Tetradecanoic acid
Palmitic acid
Stearic acid
Euxanthone mono-TMS
16.0
18.0
20.0
22.0
24.0
26.0
28.0
30.0
32.0
34.0
36.0
38.0
Retention Time (min)

New insights into the composition of Indian yellow and its use in a Rajasthani wall painting

Diego Tamburini [(1)], Charlotte Martin de Fonjaudran [(2)], Giovanni Verri [(2)], Gianluca Accorsi [(3)], Angela Acocella [(4)], Francesco Zerbetto [(4)], Amarilli Rava [(2)], Samuel Whittaker [(2)], David Saunders [(1)], Sharon Cather [(2)]

[(1)] Department of Scientific Research, The British Museum, Great Russell Street, London WC1B 3DG, UK
[(2)] The Courtauld Institute of Art, Somerset House, Strand, WC2R 0RN, London, UK,
[(3)] CNR NANOTEC - Institute of Nanotechnology c/o Campus Ecotekne, University of Salento; Via Monteroni - 73100 Lecce, Italy.
[(4)] Department of Chemistry "G.Ciamician", University of Bologna, Via F. Selmi 2, 40126, Bologna, Italy

Supplementary material

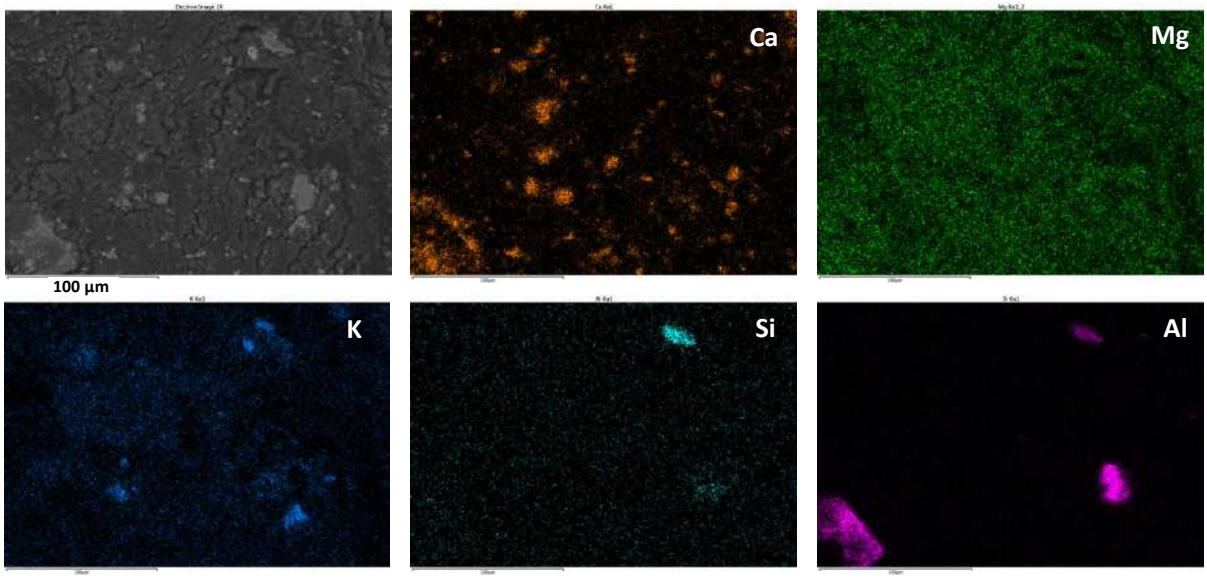

Figure S1. EDS maps obtained for the surface of the NG reference sample.

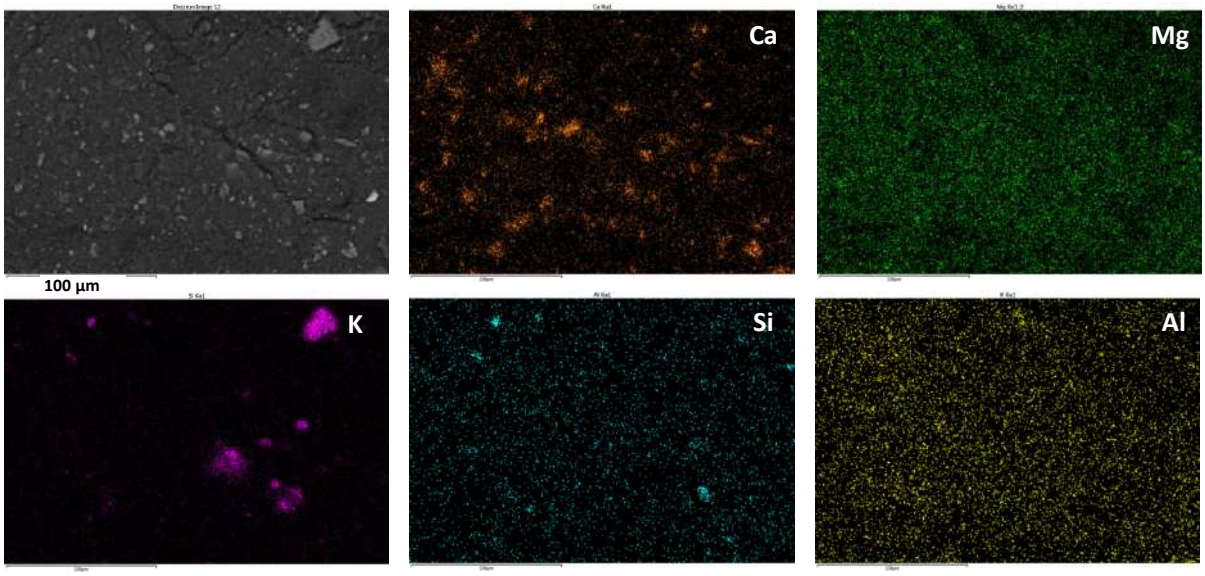

Figure S2. EDS maps obtained for the surface of the BM reference sample.

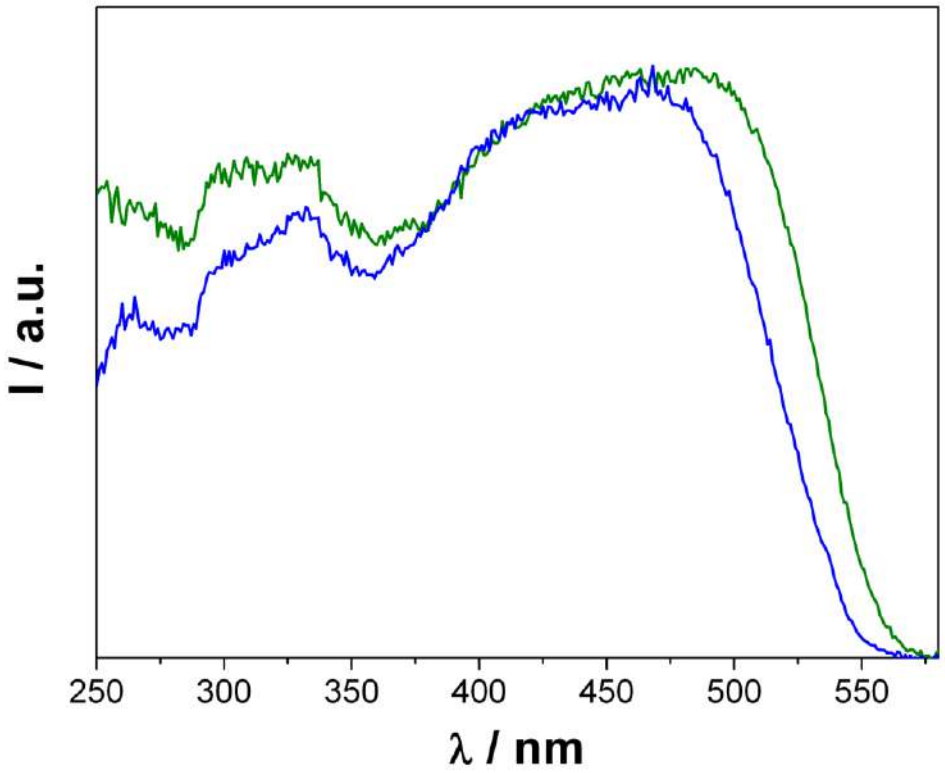

Figure S3. Normalised excitation spectra of NG (olive) and BM (blue), λ_{em} = 560 nm.

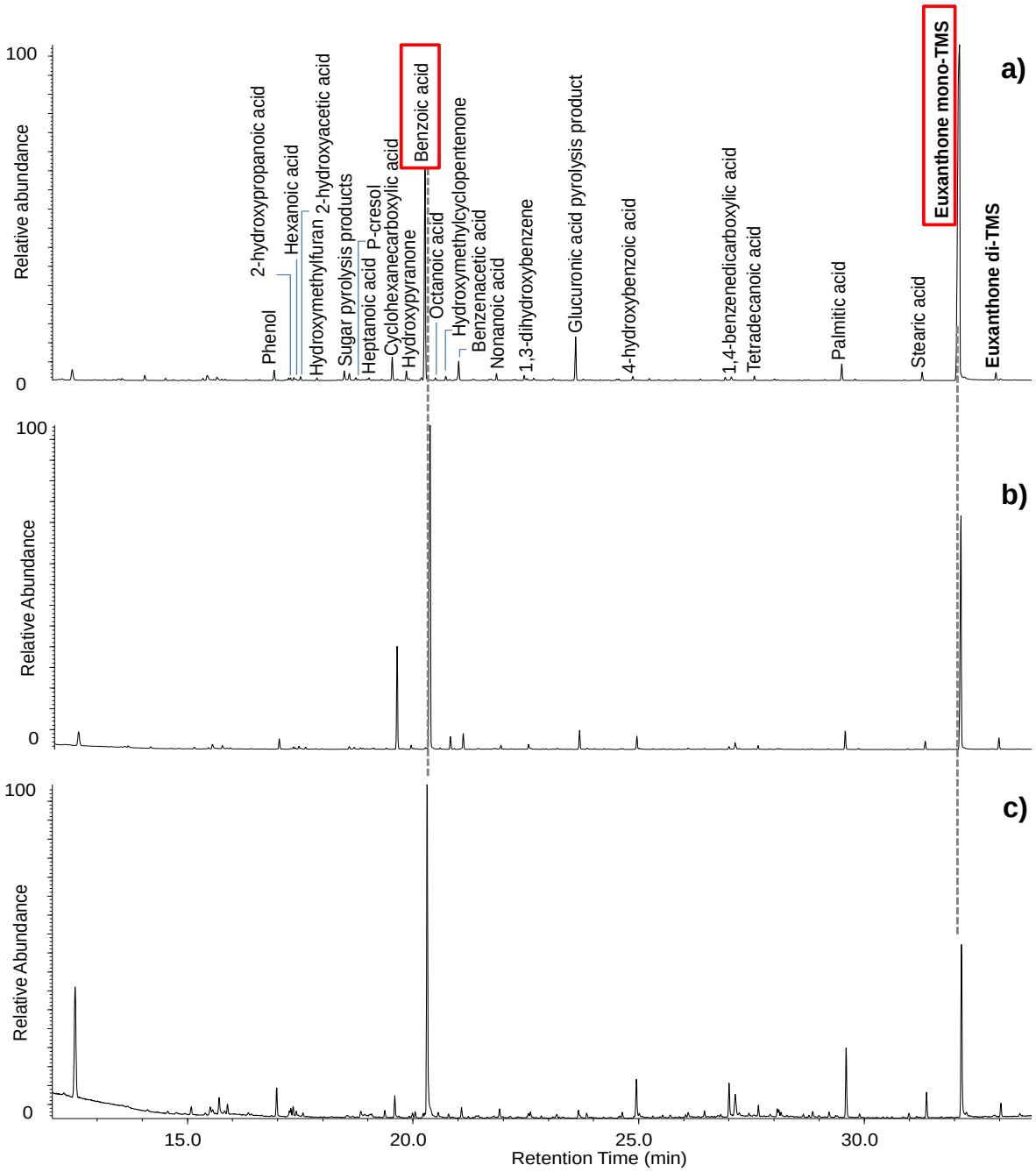

Figure S4. Total Ion Chromatograms (TICs) obtained by Py(HMD)-GC-MS analysis of the NG reference sample of Indian yellow obtained using pyrolysis temperatures **a)** 400, **b)** 500 and **c)** 600ºC

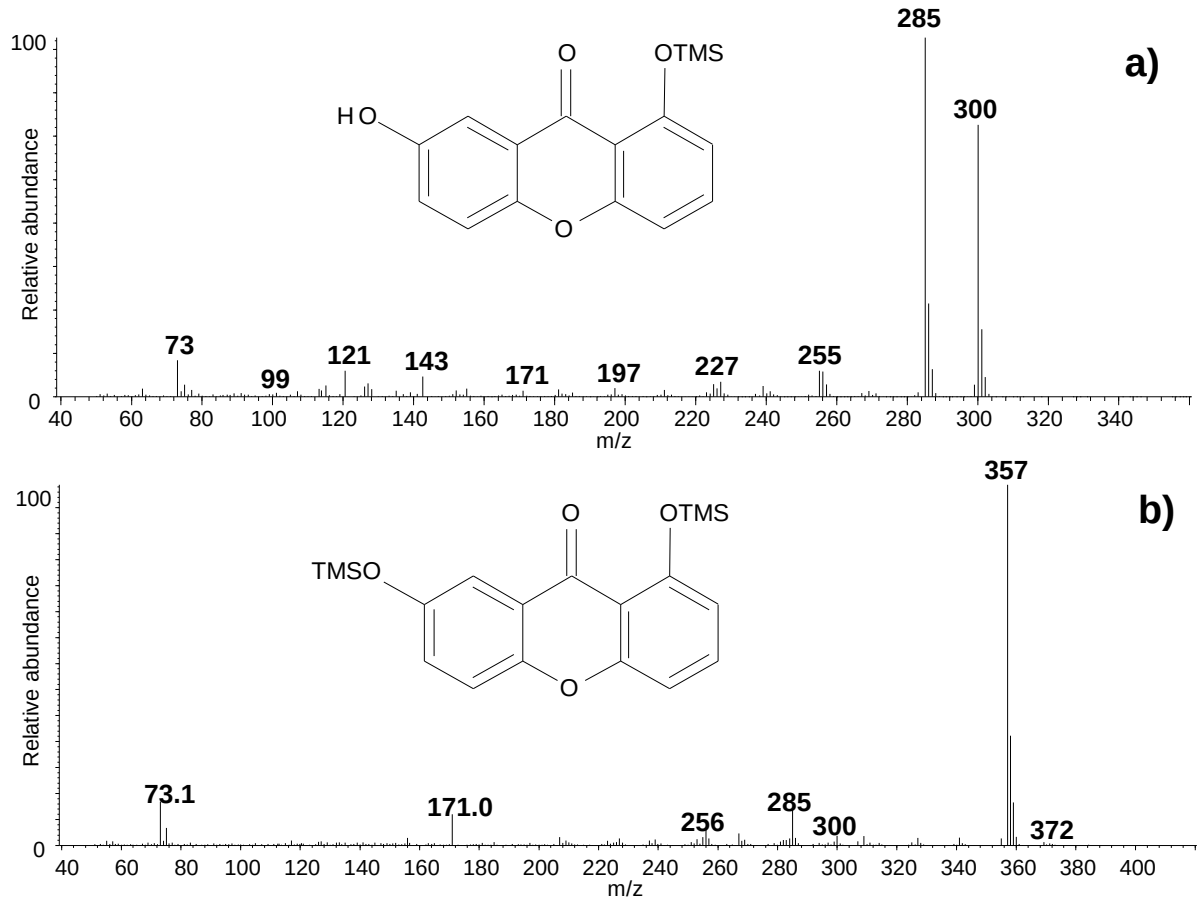

Figure S5. Mass spectra (EI) of **a)** mono-TMS and **b)** bis-TMS euxanthone.